Delayed Fluorescence

International Edition: DOI: 10.1002/anie.201710637
German Edition: DOI: 10.1002/ange.201710637

Thermally Activated Delayed Fluorescence in a $Y_3N@C_{80}$ Endohedral Fullerene: Time-Resolved Luminescence and EPR Studies

Michal Zalibera, Denis S. Krylov, Dimitrios Karagiannis, Paul-Anton Will, Frank Ziegs, Sandra Schiemenz, Wolfgang Lubitz, Sebastian Reineke,* Anton Savitsky, and Alexey A. Popov**

Abstract: *The endohedral fullerene $Y_3N@C_{80}$ exhibits luminescence with reasonable quantum yield and extraordinary long lifetime. By variable-temperature steady-state and time-resolved luminescence spectroscopy, it is demonstrated that above 60 K the $Y_3N@C_{80}$ exhibits thermally activated delayed fluorescence with maximum emission at 120 K and a negligible prompt fluorescence. Below 60 K, a phosphorescence with a lifetime of 192 ± 1 ms is observed. Spin distribution and dynamics in the triplet excited state is investigated with X- and W-band EPR and ENDOR spectroscopies and DFT computations. Finally, electroluminescence of the $Y_3N@C_{80}$/PFO film is demonstrated opening the possibility for red-emitting fullerene-based organic light-emitting diodes (OLEDs).*

Fullerenes usually exhibit low quantum yields (QY) of fluorescence (in the range of 10^{-4}) owing to the slow radiative decay and a fast and efficient inter-system crossing (ISC), leading to an almost quantitative formation of triplet states with slow non-radiative decay. Exohedral chemical derivatization can substantially modify the π-system of fullerenes and produce highly luminescent multi-adducts.[1] Another way to enhance the quantum yield of luminescence of fullerenes is based on the thermal repopulation of the S_1 state, via the T_1 state, if the S_1–T_1 gap is sufficiently small. This process is known as thermally activated delayed fluorescence (TADF) and has been found to increase the fluorescence quantum yield of C_{70} up to 0.08 at high temperatures.[2] TADF is currently an extensively examined phenomenon in the field of organic light-emitting diodes (OLEDs) as it allows to harvest up to 100% of electrically formed excitons.[3]

With the exception of several Er- and Tm-based endohedral metallofullerenes (EMFs),[4] with metal-based emission, EMFs are also non-luminescent.[5] The internal heavy-atom effect leads to even faster ISC in EMFs than in empty fullerenes. The lifetime of the S_1 state in $Sc_3N@C_{80}$ is only 48 ps.[6] Surprisingly, $Y_3N@C_{80}$ exhibits luminescence with reasonable quantum yield of ca 1% or even 8% in a cycloadduct,[7] and an unusually long luminescence lifetime of 200–800 ns at room temperature. Herein, we explore the photoemission mechanism of $Y_3N@C_{80}$ with variable-temperature time-resolved luminescence spectroscopy and EPR spectroscopy. The former reveals the evolution of the emission spectra and lifetimes with temperature, whereas the latter provides information on relaxation dynamics and spin density distribution in the triplet state of $Y_3N@C_{80}$. We show that efficient photoemission of $Y_3N@C_{80}$ is caused by the small S_1–T_1 gap leading to TADF above 60 K. In a blend with polyfluorene (PFO), $Y_3N@C_{80}$ exhibits electroluminescence, which suggests that after suitable optimization and boost of the QY, $Y_3N@C_{80}$ may be used for red or NIR-emitting OLEDs.

In deoxygenated toluene solution, $Y_3N@C_{80}$ exhibits luminescence with a QY of 1.7% and lifetime of 0.95 μs at 296 K. Saturation with air leads to a threefold reduction of the QY and appearance of singlet oxygen emission at 1270 nm. In iodobenzene, which dramatically reduces the fluorescence QY of fullerenes due to the external heavy-atom effect, only a small decrease of the QY of $Y_3N@C_{80}$ was found. The very long luminescence lifetime, dependence of the QY on oxygen, and negligible effect of the heavy atom all indicate that emission of $Y_3N@C_{80}$ is not a standard fluorescence.

Luminescence was then measured in toluene solution or in a polystyrene film at different temperatures down to 10 K. Cooling the sample from 296 K to 120 K increased the integral emission intensity (that is, the luminescence QY) more than 20-fold, but did not change the shape of the spectrum, comprising the main band at 701 nm and lower-energy vibronic bands (Figure 1a). With further cooling, a drop of the emission intensity at 701 nm was observed, and the band disappeared below 60 K (Figure 1b). At the same time, the band at 739 nm increased and became the main emission signal at low temperatures. The spectral pattern observed at 60 K remained unaltered down to 10 K (Figure 1c). The luminescence lifetime of $Y_3N@C_{80}$ dispersed in a polystyrene is gradually increasing with cooling from 1.08 μs

[*] Dr. M. Zalibera, Prof. Dr. W. Lubitz, Dr. A. Savitsky
Max Planck Institute for Chemical Energy Conversion
Stiftstr. 34–36, 45470 Mülheim an der Ruhr (Germany)
Dr. M. Zalibera
Institute of Physical Chemistry and Chemical Physics
Slovak University of Technology
Radlinského 9, 81237 Bratislava (Slovakia)
E-mail: michal.zalibera@stuba.sk
D. S. Krylov, D. Karagiannis, F. Ziegs, S. Schiemenz, Dr. A. A. Popov
Leibniz Institute for Solid State and Materials Research
Helmholtzstraße 20, 01069 Dresden (Germany)
E-mail: a.popov@ifw-dresden.de
D. Karagiannis, P.-A. Will, Prof. Dr. S. Reineke
Dresden Integrated Center for Applied Physics and Photonic Materials (IAPP) and Institute for Applied Physics (IAP), TU Dresden
Nöthnitzer Str. 61, 01187 Dresden (Germany)
E-mail: sebastian.reineke@iapp.de
Supporting information and the ORCID identification number(s) for the author(s) of this article can be found under: https://doi.org/10.1002/anie.201710637.

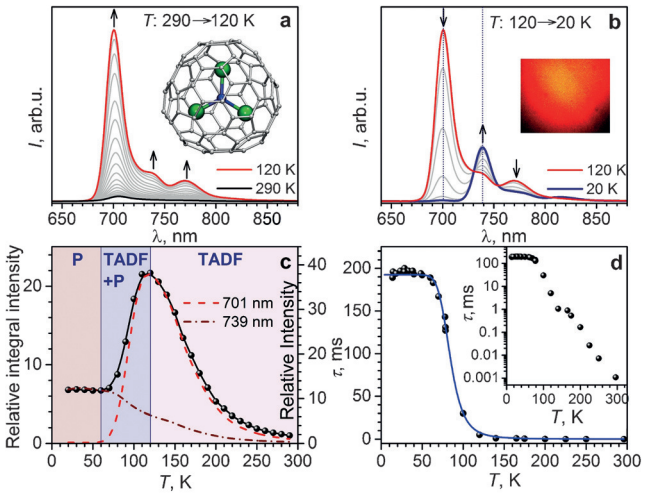

Figure 1. a),b) Luminescence spectra of $Y_3N@C_{80}$ in polystyrene film measured at 10 K steps during cooling from a) 290 K to 120 K, and b) from 120 K to 20 K; excitation at $\lambda = 405$ nm. The inset in (a) shows molecular structure of $Y_3N@C_{80}$; the inset in (b) shows a photograph of the red-emitting film at 120 K (bright spot in the centre is due to the laser). c) Temperature profiles of the relative integral emission intensity (black dots) and relative peak intensities at 701 and 739 nm (dashed lines); the values are referred to 290 K, ranges with different emission mechanisms are marked (P = phosphorescence, TADF = thermally activated delayed fluorescence); d) luminescence lifetimes of $Y_3N@C_{80}$ in polystyrene at different temperatures (the inset shows the same on a logarithmic scale); blue line is a fit to Equation (1).

at 296 K, to 1.05 ms at 140 K, and further to ca 192 ms below 60 K (Figure 1 d). A dramatic increase of the lifetime between 120 and 60 K as well as the saturation behaviour at lower temperatures parallels the changes in the emission spectra at these temperatures.

The low-temperature emission with the 192 ms lifetime is ascribed to a phosphorescence (further corroborated by EPR as discussed below). The thermally populated emission state above 60 K is then assigned to the first excited singlet state S_1. Transient absorption studies for $Y_3N@C_{80}$ have not been reported, but very fast ISC may be expected based on the 48 ps lifetime of the S_1 state in $Sc_3N@C_{80}$.[6] With such a short S_1 lifetime, it is questionable whether the prompt fluorescence of EMFs can be observed. The almost complete quenching of the fluorescence below 60 K, when thermal $T_1 \rightarrow S_1$ excitation vanishes, agrees with this reasoning and shows that prompt fluorescence of $Y_3N@C_{80}$ is negligible. Thus, the luminescence of $Y_3N@C_{80}$ above 120 K is predominantly a thermally activated delayed fluorescence, TADF. Both TADF and phosphorescence can be detected in the intermediate regime (60–120 K), whereas only phosphorescence remains below 60 K (Figure 1 c).

The S_1–T_1 energy gap, $\Delta E_{ST} = 0.09$ eV, is determined directly from the emission spectra as the energy difference between the peaks at 701 and 739 nm. Alternatively, the ΔE_{ST} gap can be estimated by fitting the temperature dependence of the luminescence lifetimes with Equation (1) (Figure 1 d):[8]

$$\tau = \frac{3 + \exp(-\Delta E_{ST}/k_B T)}{(3/\tau_{T_1}) + (1/\tau_{S_1})\exp(-\Delta E_{ST}/k_B T)} \quad (1)$$

which gives $\Delta E_{ST} = 0.08 \pm 0.01$ eV, intrinsic phosphorescence lifetime $\tau_{T_1} = 192 \pm 1$ ms, and $\tau_{S_1} = 1.7 \pm 1.3$ μs.

TADF has been described for empty fullerenes, and is particularly well studied for C_{70}.[2,9] In comparison to $Y_3N@C_{80}$, empty fullerenes have much higher ΔE_{ST} values (0.25–0.30 eV), which result in higher temperatures, at which TADF is efficient (for example, above 250 K in C_{70}).

To understand the origin of the small ΔE_{ST} gap in $Y_3N@C_{80}$, we performed DFT calculations.[10] In the lowest energy configuration of $Y_3N@C_{80}$, Y atoms coordinate cage hexagons in η^6-manner (Figure 2). The HOMO of the molecule is localized on the poles, whereas the LUMO has the largest contributions near the Y-coordinated hexagons. Time-dependent DFT calculations show that $S_0 \rightarrow S_1$ excitation is predominantly the HOMO–LUMO transition and can be described as the intramolecular electron transfer from the poles to the equator (see the difference electron density in Figure 2 c). The spatial separation of the "donor" and "acceptor" parts causes the low S_1–T_1 gap (0.079 eV at the TD-PBE/TZ2P level). Importantly, Y_3N cluster has a negligible contribution to the $S_0 \rightarrow S_1$ excitation. Likewise, the spin density in the T_1 triplet state is localized on the carbon cage with very small spin populations on Y and N (Figure 2 d).

$Y_3N@C_{80}$ was further studied by electron paramagnetic resonance (EPR) spectroscopy. The long triplet lifetime enables the use of light-induced EPR to study the spin density distribution and relaxation dynamics of the triplet $^3Y_3N@C_{80}$*. Under continuous laser illumination below 120 K in frozen toluene or polystyrene film, a continuous wave (CW) EPR signal of the $^3Y_3N@C_{80}$* triplet is measured (Supporting Information, Figure S1), which also features

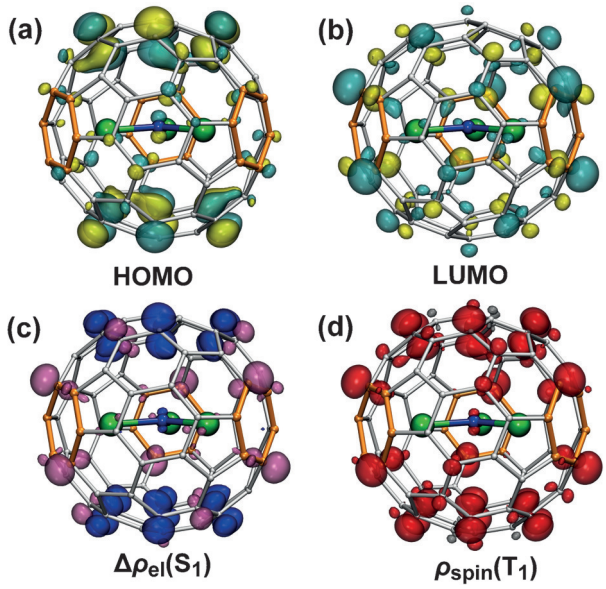

Figure 2. a) HOMO and b) LUMO of $Y_3N@C_{80}$ with C_3-configuraton (plane of the cluster and C_3 axis are normal and parallel to the paper plane, respectively); c) TD-DFT computed difference electron density for the $S_0 \rightarrow S_1$ excitation (purple "+"/blue "−"); d) Spin density distribution in the T_1 triplet state of $Y_3N@C_{80}$. Carbon atoms are grey except for metal-coordinated hexagons shown in orange, Y green, N blue.

a half-field signal at helium temperatures (Supporting Information, Figure S1).

A further characterization of $^3Y_3N@C_{80}$* was achieved in a multifrequency pulsed EPR study. Figure 3 shows the time-resolved electron spin echo detected EPR (TR-ESE-EPR) spectra of the $Y_3N@C_{80}$ triplet at X- and W-band microwave frequencies. Shortly after the laser flash (Figure 3 a,d) the spectra exhibit polarized character owing to the non-equilibrium population of the triplet energy levels generated during the intersystem crossing from the S_1 state.[11] The polarization pattern is described as EE/AA at both microwave frequencies (emission/absorption). The polarization pattern is opposite to that observed for the empty fullerene excited triplets $^3C_{60}$*, $^3C_{70}$* (AA/EE).[12] The equilibrium population of the triplet energy levels is accomplished via spin lattice relaxation approximately 500 µs after the laser flash at 20 K (Figure 3 g, T_1 of 74 µs and 91 µs at X- and W-band, respectively). EPR spectra recorded with longer delay after flash (t_{DAF}) correspond to the Boltzmann population at the corresponding temperature (Figure 3 b,e), and are reproduced in a simulation with a rhombic g tensor ($g_x = 2.0004$, $g_y = 2.0008$, $g_z = 2.0030$) and an axially symmetric zero field splitting tensor (ZFS, $D = +128$ MHz, $E = 0$). The positive sign of D is determined by utilizing the enhanced thermal spin polarization in W-band EPR (Supporting Information, Figures S2, S3). The g tensor of $^3Y_3N@C_{80}$* is more asymmetric and the ZFS is smaller than in the case of the empty fullerene $^3C_{60}$* ($D/E = -340/+15$ MHz),[12a] $^3C_{70}$* ($D/E = +153/+5$–42 MHz)[12b,c] and monometallo endohedral fullerenes $^3Sr@C_{74}$* ($|D|/|E| = 260/35$ MHz), $^3Ba@C_{74}$* ($|D|/|E| = 250/47$ MHz),[13] and nonmetal endofullerene $^3H_2@C_{60}$* ($D/E \approx -340/+15$ MHz).[14] The small ZFS in $^3Y_3N@C_{80}$* points to a negligible impact of the spin orbit coupling and is thus in line with the dominant spin density distribution on the carbon cage (Figure 2 d). It also reflects the larger size of the cage and thus formally larger spin-spin distance between the unpaired electrons.

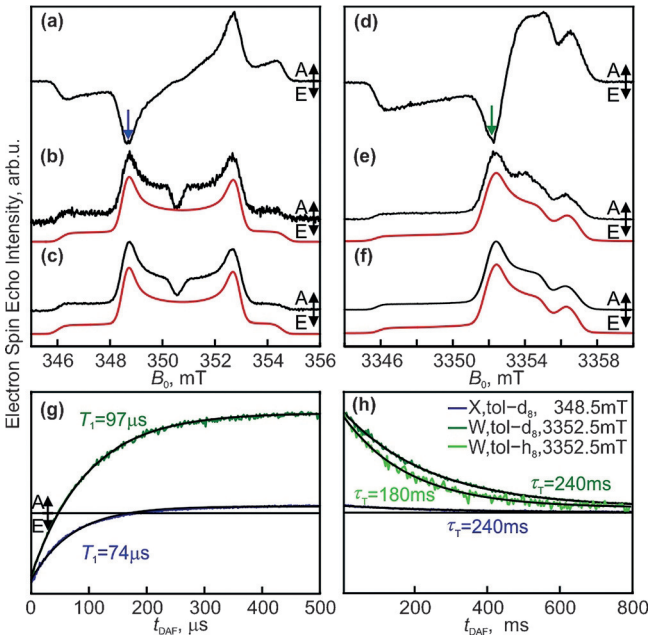

Figure 3. a)–c) X-band and d)–f) W-band ESE detected EPR spectra of the $Y_3N@C_{80}$ excited triplet ($^3Y_3N@C_{80}$*) in frozen [D_8]toluene solution at 20 K: a),d) with delay after the 488 nm laser pulse $t_{DAF} = 500$ ns, b),e) $t_{DAF} = 15$ ms, and c),f) continuous 510 nm laser illumination. Red lines represent EPR spectra calculated using the spin Hamiltonian parameters discussed in the text. g),h) ESE intensity of the emissive polarized signal of the $^3Y_3N@C_{80}$* at X- and W-band at 20 K as a function of t_{DAF} (arrows in (a) and (d) mark the field position of time recordings). The polarization of the signal decays with the spin lattice relaxation time T_1 (g) followed by the decay of the Boltzmann-population signal according to the triplet lifetime τ_{T_1} (h). τ_{T_1} values differ in protonated (180 ms) and deuterated (240 ms) toluene matrix.

TR-ESE-EPR shows that the $^3Y_3N@C_{80}$* exhibits a long lifetime (τ_{T_1}) depending on the deuteration level of toluene (Figure 3 h; 240 ms in [D_8]toluene and 180 ms in [H_8]toluene at 20 K). Thus, the τ_{T_1} values determined by TR-ESE-EPR are in good agreement with the lifetime obtained from the luminescence (192 ms in polystyrene). Owing to the long lifetime of the T_1 at 20 K, the pulsed EPR spectra obtained under continuous irradiation (Figure 3 c,f) correspond to the signals with equilibrium population of the triplet energy levels, and can be well simulated using the spin Hamiltonian parameters derived above. The X-band spectra (Figure 3 b,c) exhibit an additional narrow hole in the centre of the spectrum, which can be traced back to the simultaneous excitation of both allowed electron spin transitions of the triplet ($T_0 \leftrightarrow T_+$ and $T_0 \leftrightarrow T_-$) as described for $^3C_{70}$.[12c]

The detailed image of the spin density distribution in the T_1 state is encoded in the hyperfine interactions of the electrons with the nearby nuclei, and can be extracted using hyperfine spectroscopy methods such as electron nuclear double resonance (ENDOR).[15] ENDOR proved very powerful in investigations of paramagnetic endohedral fullerenes $La@C_{82}$,[16] $N@C_{60}$,[17] $N@C_{70}$,[18] and the triplet excited state of $H_2@C_{60}$.[14] For light excited triplets ENDOR studies are scarce and often hampered by the short τ_{T_1} and/or short T_1 relaxation times. Here, the long τ_{T_1} of $^3Y_3N@C_{80}$* allowed for a detailed ENDOR investigation. W-band ENDOR spectra recorded at different field positions corresponding to the turning points of the ZFS pattern, are shown in Figure 4. The trace in Figure 4 a shows intense sharp lines around 7 MHz, 21.9 MHz and 35.9 MHz, at the Larmor frequencies of the ^{89}Y, ^2H and ^{13}C nuclei. These signals are characteristic for the triplet states and originate from degenerate NMR transitions within the zero level electron spin manifold $m_S = 0$. The additional broader lines at frequencies below 13.0 MHz reflect the hyperfine and quadrupole couplings of the cluster nuclei, ^{89}Y and ^{14}N (Figure 4 c,d; Supporting Information, Figure S4). The orientation selection achieved in the W-band ENDOR spectra reveal a predominantly isotropic character of the ^{89}Y hyperfine interaction, with a small positive $A_{iso}(^{89}Y)$ hyperfine coupling (hfc) constant of +1.02 MHz, (for details, see the Supporting Information). The three Y nuclei in the cluster are magnetically equivalent. A small positive axial hfc with $A_{\parallel}(^{14}N) = +0.62$ MHz, $A_{\perp}(^{14}N) = +0.15$ MHz ($A_{iso}(^{14}N) = +0.46$ MHz), and a somewhat larger nuclear quadrupole coupling of $|e^2Qq/h| = 1.46$ MHz (asymmetry $\eta \approx 0$), is found for the central ^{14}N atom. Experimental hfc values are in reasonable agreement with the results of DFT calculations in the Supporting Information.

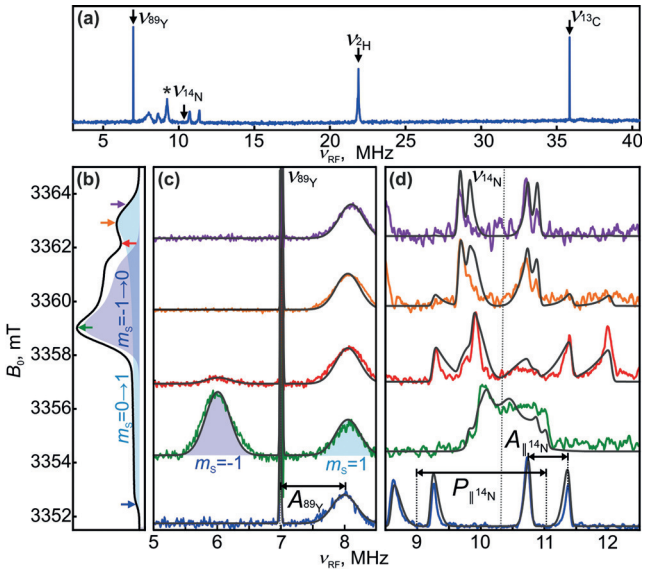

Figure 4. a) W-band ^{14}N Mims-ENDOR spectrum of $^3Y_3N@C_{80}$* recorded under continuous illumination (510 nm) at 20 K. The Larmor frequencies of nuclei in the system are labelled by arrows (* marks an artefact line). The spectrum was obtained at the field position marked by the blue arrow in the ESE detected EPR spectrum shown in (b). c),d) The orientation selected ^{89}Y (c) and ^{14}N (d) ENDOR spectra obtained at field positions marked by identically coloured arrows in (b). Grey lines show spectra calculated using the spin Hamiltonian parameters from the Supporting Information, Table S1. The splitting due to the corresponding hyperfine (*A*) and quadrupolar (*P*) interactions are indicated.

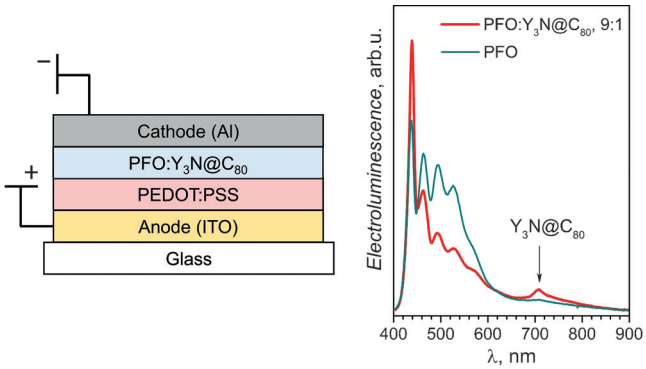

Figure 5. Principle of the OLED device (left) and comparison of the electroluminescence of the PFO and PFO:$Y_3N@C_{80}$ films (right) at room temperature.

The isotropic hfc constants translate to about 0.082 % s-spin population at each Y atom and 0.025 % s-spin population on the nitrogen, respectively, in line with the negligible spin density delocalization on the cluster (Figure 2 d). In the family of Y-containing EMF-radicals a similar situation is found for $Y@C_{82}$ with $A_{iso}(^{89}Y)$ of 1.33 MHz (0.1 % s-spin pop.).[19] Somewhat larger metal contributions are found in the radical anion of $Y_3N@C_{80}$ (32 MHz) and its pyrrolidine adduct (17.5 and 2×3.8 MHz).[20] A strikingly different situation is found for the unpaired electron delocalized between two Y atoms in $Y_2@C_{79}N$ and $Y_2@C_{80}(CH_2C_6H_5)$ with $A_{iso}(^{89}Y)$ close to 220 MHz (17.6 % s-spin pop. for each Y).[21] $A_{iso}(^{14}N)$ values reported earlier for nitride clusterfullerenes are 3.7 MHz in the anion radical of $Y_3N@C_{80}$ and 1.4 MHz in its pyrrolidine adduct.[20]

TADF has recently been proposed as third generation emitter concept since it allows all triplets to be harvested radiatively and thus the internal quantum efficiency approaches 100 %. To verify the applicability of EMFs such as $Y_3N@C_{80}$ in TADF-OLEDs, we prepared a simple solution-processed device using $Y_3N@C_{80}$-embedded in a polyfluorene (PFO) as an active material (Figure 5). The poly(3,4-ethylenedioxythiophene) polystyrene sulfonate (PEDOT:PSS) and PFO:$Y_3N@C_{80}$ layers were prepared sequentially by spin-coating onto indium tin oxide (ITO) electrodes. The device was then transferred into a vacuum chamber for Al deposition. Figure 5 shows that PFO with 10 % mass of $Y_3N@C_{80}$ has a new band at 708 nm owing to the electroluminescence of $Y_3N@C_{80}$, which is absent in the device made from pure PFO. The quantum yield of $Y_3N@C_{80}$ is rather low at room temperature for an efficient application, but a further increase of the QY may be achieved via derivatization,[7b] by changing the temperature (Figure 1), or by supramolecular assemblies.[22] A co-existence of PFO fluorescence and $Y_3N@C_{80}$ luminescence in Figure 5 also indicates that the energy transfer in this device is not very efficient and needs further optimization.

To summarize, we have discovered that $Y_3N@C_{80}$ has a small S_1-T_1 gap of 0.08–0.09 eV and exhibits thermally activated delayed fluorescence above 60 K, with a quantum yield increasing from about 1 % at room temperature to the maximum value of about 22 % at 120 K. Below 60 K, phosphorescence with a long lifetime of 192 ± 1 ms is exclusively observed. The triplet state of $Y_3N@C_{80}$ is extensively characterized by time-resolved EPR and ENDOR spectroscopy, providing information on the dynamics, hyperfine structure, and spin density distribution in the T_1 state.

Acknowledgements

The authors acknowledge the European Research Council (ERC) under the European Union's Horizon 2020 research and innovation programme (grant No 648295 "GraM3"), Slovak Research and Development Agency (APVV-15-0053), Slovak Scientific Grant Agency VEGA (1/0416/17), and the Max Planck Society. Computational resources were provided by the Center for High Performance Computing at the TU Dresden.

Conflict of interest

The authors declare no conflict of interest.

Keywords: delayed fluorescence · endohedral fullerenes · EPR/ENDOR · luminescence · OLEDs

How to cite: *Angew. Chem. Int. Ed.* **2018**, *57*, 277–281
Angew. Chem. **2018**, *130*, 283–287

[1] a) K. P. Castro, Y. Jin, J. J. Rack, S. H. Strauss, O. V. Boltalina, A. A. Popov, *J. Phys. Chem. Lett.* **2013**, *4*, 2500 – 2507; b) Y. Matsuo, Y. Sato, M. Hashiguchi, K. Matsuo, E. Nakamura, *Adv. Funct. Mater.* **2009**, *19*, 2224 – 2229; c) N. Lou, Y. Li, L. Gan, *Angew. Chem. Int. Ed.* **2017**, *56*, 2403 – 2407; *Angew. Chem.* **2017**, *129*, 2443 – 2447.

[2] M. N. Berberan-Santos, J. M. M. Garcia, *J. Am. Chem. Soc.* **1996**, *118*, 9391 – 9394.

[3] a) Z. Yang, Z. Mao, Z. Xie, Y. Zhang, S. Liu, J. Zhao, J. Xu, Z. Chi, M. P. Aldred, *Chem. Soc. Rev.* **2017**, *46*, 915 – 1016; b) Y. Tao, K. Yuan, T. Chen, P. Xu, H. Li, R. Chen, C. Zheng, L. Zhang, W. Huang, *Adv. Mater.* **2014**, *26*, 7931 – 7958; c) H. Uoyama, K. Goushi, K. Shizu, H. Nomura, C. Adachi, *Nature* **2012**, *492*, 234 – 238; d) S. Reineke, *Nat. Photonics* **2014**, *8*, 269 – 270.

[4] a) Z. Wang, N. Izumi, Y. Nakanishi, T. Koyama, T. Sugai, M. Tange, T. Okazaki, H. Shinohara, *ACS Nano* **2016**, *10*, 4282 – 4287; b) Y. Ito, T. Okazaki, S. Okubo, M. Akachi, Y. Ohno, T. Mizutani, T. Nakamura, R. Kitaura, T. Sugai, H. Shinohara, *ACS Nano* **2007**, *1*, 456 – 462; c) R. M. Macfarlane, D. S. Bethune, S. Stevenson, H. C. Dorn, *Chem. Phys. Lett.* **2001**, *343*, 229 – 234.

[5] A. A. Popov, S. Yang, L. Dunsch, *Chem. Rev.* **2013**, *113*, 5989 – 6113.

[6] a) J. R. Pinzón, C. M. Cardona, M. A. Herranz, M. E. Plonska-Brzezinska, A. Palkar, A. J. Athans, N. Martin, A. Rodriguez-Fortea, J. M. Poblet, G. Bottari, T. Torres, S. Shankara Gayathri, D. M. Guldi, L. Echegoyen, *Chem. Eur. J.* **2009**, *15*, 864 – 877; b) J. R. Pinzón, M. E. Plonska-Brzezinska, C. M. Cardona, A. J. Athans, S. S. Gayathri, D. M. Guldi, M. A. Herranz, N. Martin, T. Torres, L. Echegoyen, *Angew. Chem. Int. Ed.* **2008**, *47*, 4173 – 4176; *Angew. Chem.* **2008**, *120*, 4241 – 4244.

[7] a) L. Bharadwaj, L. Novotny, *J. Phys. Chem. C* **2010**, *114*, 7444 – 7447; b) K. Toth, J. K. Molloy, M. Matta, B. Heinrich, D. Guillon, G. Bergamini, F. Zerbetto, B. Donnio, P. Ceroni, D. Felder-Flesch, *Angew. Chem. Int. Ed.* **2013**, *52*, 12303 – 12307; *Angew. Chem.* **2013**, *125*, 12529 – 12533.

[8] M. J. Leitl, F.-R. Küchle, H. A. Mayer, L. Wesemann, H. Yersin, *J. Phys. Chem. A* **2013**, *117*, 11823 – 11836.

[9] a) C. Baleizão, S. Nagl, S. M. Borisov, M. Schaferling, O. S. Wolfbeis, M. N. Berberan-Santos, *Chem. Eur. J.* **2007**, *13*, 3643 – 3651; b) C. Baleizão, M. N. Berberan-Santos, *J. Chem. Phys.* **2007**, *126*, 8; c) F. A. Salazar, A. Fedorov, M. N. Berberan-Santos, *Chem. Phys. Lett.* **1997**, *271*, 361 – 366; d) S. M. Bachilo, A. F. Benedetto, R. B. Weisman, J. R. Nossal, W. E. Billups, *J. Phys. Chem. A* **2000**, *104*, 11265 – 11269; e) S. Kochmann, C. Baleizão, M. N. Berberan-Santos, O. S. Wolfbeis, *Anal. Chem.* **2013**, *85*, 1300 – 1304; f) C. Baleizão, M. N. Berberan-Santos, *Ann. N. Y. Acad. Sci.* **2008**, *1130*, 224 – 234.

[10] a) D. N. Laikov, Y. A. Ustynuk, *Russ. Chem. Bull.* **2005**, *54*, 820 – 826; b) F. Neese, *WIREs Comput. Mol. Sci.* **2012**, *2*, 73 – 78; c) D. A. Pantazis, X.-Y. Chen, C. R. Landis, F. Neese, *J. Chem. Theory Comput.* **2008**, *4*, 908 – 919; d) F. Neese, *J. Chem. Phys.* **2005**, *122*, 034107.

[11] *Introduction to Dynamic Spin Chemistry: Magnetic Field Effects upon Chemical and Biochemical Reactions* (Ed.: H. Hayashi), World Scientific Publishers, Singapore, **2003**.

[12] a) X. L. R. Dauw, G. J. B. van den Berg, D. J. van den Heuvel, O. G. Poluektov, E. J. J. Groenen, *J. Chem. Phys.* **2000**, *112*, 7102 – 7110; b) X. L. R. Dauw, O. G. Poluektov, J. B. M. Warntjes, M. V. Bronsveld, E. J. J. Groenen, *J. Phys. Chem. A* **1998**, *102*, 3078 – 3082; c) M. N. Uvarov, L. V. Kulik, T. I. Pichugina, S. A. Dzuba, *Spectrochim. Acta Part A* **2011**, *78*, 1548 – 1552.

[13] O. Haufe, M. Hecht, A. Grupp, M. Mehring, M. Jansen, *Z. Anorg. Allg. Chem.* **2005**, *631*, 126 – 130.

[14] V. Filidou, S. Mamone, S. Simmons, S. D. Karlen, H. L. Anderson, C. W. M. Kay, A. Bagno, F. Rastrelli, Y. Murata, K. Komatsu, X. Lei, Y. Li, N. J. Turro, M. H. Levitt, J. J. L. Morton, *Philos. Trans. R. Soc. London Ser. A* **2013**, *371*, 20120475.

[15] A. Schweiger, G. Jeschke, *Principles of Pulse Electron Paramagnetic Resonance Spectroscopy*, Oxford University Press, **2001**.

[16] a) K. P. Dinse, T. Kato in *Novel NMR and EPR Techniques, Lect. Notes Phys. 684* (Eds.: J. Dolinšek, M. Vilfan, S. Žumer), Springer, Berlin, **2006**, pp. 185 – 207; b) N. Weiden, T. Kato, K. P. Dinse, *J. Phys. Chem. B* **2004**, *108*, 9469 – 9474; c) V. K. Koltover, V. P. Bubnov, Y. I. Estrin, V. P. Lodygina, R. M. Davydov, M. Subramoni, P. T. Manoharan, *Phys. Chem. Chem. Phys.* **2003**, *5*, 2774 – 2777.

[17] a) A. M. Tyryshkin, J. J. L. Morton, A. Ardavan, S. A. Lyon, *J. Chem. Phys.* **2006**, *124*, 234508; b) C. Knapp, N. Weiden, K. P. Dinse, *Magn. Reson. Chem.* **2005**, *43*, S199 – S204.

[18] N. Weiden, B. Goedde, H. Kass, K. P. Dinse, M. Rohrer, *Phys. Rev. Lett.* **2000**, *85*, 1544 – 1547.

[19] S. Knorr, A. Grupp, M. Mehring, U. Kirbach, A. Bartl, L. Dunsch, *Appl. Phys. A* **1998**, *66*, 257 – 264.

[20] a) L. Echegoyen, C. J. Chancellor, C. M. Cardona, B. Elliott, J. Rivera, M. M. Olmstead, A. L. Balch, *Chem. Commun.* **2006**, 2653 – 2655; b) C. Zhao, T. Wang, Y. Li, H. Meng, M. Nie, J. Tian, C.-R. Wang, *Phys. Chem. Chem. Phys.* **2017**, *19*, 26846 – 26850.

[21] a) T. Zuo, L. Xu, C. M. Beavers, M. M. Olmstead, W. Fu, T. D. Crawford, A. L. Balch, H. C. Dorn, *J. Am. Chem. Soc.* **2008**, *130*, 12992 – 12997; b) F. Liu, D. S. Krylov, L. Spree, S. M. Avdoshenko, N. A. Samoylova, M. Rosenkranz, A. Kostanyan, T. Greber, A. U. B. Wolter, B. Büchner, A. A. Popov, *Nat. Commun.* **2017**, *8*, 16098.

[22] O. Kozák, M. Sudolská, G. Pramanik, P. Cígler, M. Otyepka, R. Zbořil, *Chem. Mater.* **2016**, *28*, 4085 – 4128.

Manuscript received: October 15, 2017
Accepted manuscript online: November 9, 2017
Version of record online: December 8, 2017

